Materials Chemistry and Physics 189 (2017) 90–95

Contents lists available at ScienceDirect

Materials Chemistry and Physics

journal homepage: www.elsevier.com/locate/matchemphys

Investigation of structural, electronic and anisotropic elastic properties of *Ru*-doped WB_2 compound by increased valence electron concentration

Gokhan Surucu [a, b, *], Cagil Kaderoglu [c], Engin Deligoz [d], Haci Ozisik [d]

[a] Ahi Evran University, Department of Electric and Energy, 40100, Kirsehir, Turkey
[b] Gazi University, Photonics Application and Research Center, 06500, Ankara, Turkey
[c] Ankara University, Department of Engineering Physics, 06100, Ankara, Turkey
[d] Aksaray University, Department of Physics, 68100, Aksaray, Turkey

HIGHLIGHTS

- Effects of Ru substitution in WB_2 using increased valence electron concentration.
- Structural, electronic, mechanic and elastic properties for increasing *Ru* content.
- Considered alloys are incompressible, brittle, stiffer and high hard materials.

ARTICLE INFO

Article history:
Received 22 September 2016
Received in revised form
4 December 2016
Accepted 12 December 2016
Available online 13 December 2016

Keywords:
$W_{1-x}Ru_xB_2$
Density functional theory (DFT)
Anisotropy
Mechanical properties
Electronic structure
Site occupancy

ABSTRACT

First principles density functional theory (DFT) calculations have been used to investigate the structural, anisotropic elastic and electronic properties of ruthenium doped tungsten-diboride ternary compounds ($W_{1-x}Ru_xB_2$) for an increasing molar fraction of Ru atom from 0.1 to 0.9 by 0.1. Among the nine different compositions, $W_{0.3}Ru_{0.7}B_2$ has been found as the most stable one due to the formation energy and band filling theory calculations. Moreover, the band structures and partial density of states (PDOS) have been computed for each *x* composition. After obtaining the elastic constants for all *x* compositions, the secondary results such as Bulk modulus, Young's modulus, Poisson's ratio, Shear modulus, and Vickers Hardness of polycrystalline aggregates have been derived and the relevant mechanical properties have been discussed. In addition, the elastic anisotropy has been visualized in detail by plotting the directional dependence of compressibility, Poisson ratio, Young's and Shear moduli.

1. Introduction

Super-hard materials (SHM) are important for their wide usage area from cutting and polishing tools to wear and scratch resistant coatings [1–3]. Since diamond and cubic boron nitride failed to satisfy the need of some emerging industrial applications, most studies have been focused on the combination of transition metals (TM) with light elements to design new SHMs [4–6]. Here, while the high valence electron density of the heavy TM atom leads to a high bulk modulus which causes high incompressibility due to the greater repulsive forces within the material; the light element of the compound provides strong covalent bonding network in the structure which is responsible for the elastic and plastic deformation resistance [7–10]. In accordance with this designing strategy, carbides, oxides, nitrides and borides of TMs have been in the center of interest to meet the requirements of new technologies [1,5,11,12]. The physical and chemical properties of these alloys such as high melting point, excellent oxidation resistance, lower diffusion coefficient, good thermal and electrical conductivity are unique [13,14]. However, only borides among these groups are easy to synthesize under ambient temperature and pressure [5,15].

Especially, tungsten-boron combinations, which constitute an important group of ceramics, have become prominent among all other TM borides due to their relative inexpensiveness [8]. Hence,

* Corresponding author. Ahi Evran University, Department of Electric and Energy, 40100, Kirsehir, Turkey.
E-mail address: g_surucu@yahoo.com (G. Surucu).

http://dx.doi.org/10.1016/j.matchemphys.2016.12.036
0254-0584/

many theoretical and experimental works have been done for different combinations including W_2B, WB, WB_2, W_2B_5, WB_4, WB_{12}, W_8B_7 and W_2B_3 phases [8,9,16–22]. Among these, P6$_3$/mmc-WB_2 phase has come to the forefront as a candidate to replace the traditional SHMs due to its high hardness and incompressibility values [21,22].

Recent works have started to discuss whether another TM atom addition induces a change in the microstructure of the ceramic to improve its mechanical properties. For example, Mohammadi et al. [15] have examined molybdenum addition into the WB_4 by arc melting method while Akopov et al. [23] have done a similar work with titanium, zirconium and hafnium metals. Also, the experimental work done by Yeung et al. [10] and the theoretical work done by Feng et al. [24] have reported the addition of tantalum and rhenium into the WB and W_2B_5 phases, respectively. As for WB_2 phase, besides the work of Cao et al. [25] in which nickel doping have been studied experimentally, two other theoretical studies have been done by Surucu et al. [26] and Euchner et al. [6] for technetium, aluminum, titanium and vanadium dopants. As can be seen from above-mentioned studies, adding another TM atom into the tungsten-boride systems has an improving impact on the mechanical properties of these materials. Also, other works done for similar systems support the same doping strategy [27–30].

Consequently, finding optimal doping rates of different TM atoms into TM borides can be helpful to design new materials in parallel with the technological requirements. Based on this idea and above-stated studies, we have decided to introduce ruthenium as an additive to WB_2 phase due to the high performance of Ru–B systems as hard materials [31–33]. Moreover, ruthenium is the least compressible element in its own row of the periodic table [7]. Also, it has a high bulk modulus, namely a high valence electron concentration (VEC) [34]. Therefore we nominate it as a suitable dopant to the WB_2.

To the best of our knowledge, there is only one experimental work done by Rogl et al., in 1970 for $x = 0.7$ composition [35]. Crystal structure of $W_{0.3}Ru_{0.7}B_2$ was investigated in this work, but mechanical and electronic properties of the $W_{1-x}Ru_xB_2$ are still missing. In this context, we aim to study the detailed structural, electronic and anisotropic elastic properties of $W_{1-x}Ru_xB_2$ compounds ($x = 0.1$–0.9) as a function of increased VEC using first principle calculations for the first time in the literature.

2. Calculation methods

All of the simulations in this work were performed by the self-consistent density functional theory (DFT) with a plane-wave pseudopotential approach implemented in the CASTEP code [36,37]. Perdew-Burke-Ernzerhof (PBE) parametrization of the generalized gradient approximation (GGA) was used for the exchange-correlation terms in the electron–electron interaction [38,39]. The interactions between the ions and the electrons were described by using the Ultrasoft Vanderbilt pseudopotential [40]. The electronic valence configurations for each atomic species were chosen as W:$5s^25p^65d^46s^2$, Ru:$4s^24p^6\ 4d^75s^1$, and B:$2s^22p^1$ within the virtual crystal approximation (VCA) [41]. The electronic wave functions were expanded in the plane waves up to a 500 eV kinetic energy cutoff. Self-consistent solutions were obtained by employing a set ($20 \times 20 \times 8$) Monkhorst–Pack [42] grid of k-points in the irreducible Brillouin zone. The molar fraction (x) of Ru atom in the structure was increased from 0.1 to 0.9 by 0.1 maintaining an integer number of electrons per unit cell. The VEC numbers were calculated using the following Formula (1), where valence electron numbers of constituent atoms are 6 for W, 8 for Ru, and 3 for B.

$$\mathrm{VEC} = \frac{[(1-\mathrm{x}).\mathrm{W} + \mathrm{x}.\mathrm{Ru} + 2.\mathrm{B}]}{3} \quad (1)$$

In addition, spin-polarization effect was also taken into account to determine whether there is a difference between the results. However, no significant difference was observed between spin- and nonspin-polarized calculations.

3. Results and discussion

3.1. Structural and electronic properties

In our calculations, $W_{1-x}Ru_xB_2$ compounds have been modeled to find the most stable structure for increasing doping rates of Ru atom. Within this framework, molar fraction x has been increased from 0.1 to 0.9 by 0.1 steps while keeping the well-known P6$_3$/mmc (space group:194) symmetry of the host WB_2 [17,20,43]. In this structure, TM atoms occupy $2c$ sites (1/3, 2/3, 1/4), while B atoms occupy $4f$ sites (1/3, 2/3, z). The optimized lattice parameters and the VEC values calculated according to the Formula (1) as a function of x composition are given in Table 1 and shown in Fig. 1. The dashed lines in this figure correspond to a linear and biquadratic equation, obtained from least squares fitting, for a and c parameters, respectively. As can be seen from this table and figure, increasing VEC and x content leads to an almost linear decrease in the optimized lattice parameter c while the lattice parameter a exhibits a downward bowing with a minimum point at $x = 0.7$. This deviation of a from Vegard's Law [44], which was also similarly observed for $Os_xW_{1-x}B_2$ [30], might be attributed to the mismatch of the lattice constants of WB_2 and RuB_2 sublattices.

The formation energy (ΔH_f) of the present system has been calculated using the following Formula (2) and listed in Table 1 for each x value.

$$\mathrm{E}^{\mathrm{W_{1-x}Ru_xB_2}}_{\mathrm{formation}} = \mathrm{E}^{\mathrm{W_{1-x}Ru_xB_2}}_{\mathrm{total}} - \left[(1-\mathrm{x})\mathrm{E}^{\mathrm{W}}_{\mathrm{solid}} + \mathrm{xE}^{\mathrm{Ru}}_{\mathrm{solid}} + 2\mathrm{E}^{\mathrm{B}}_{\mathrm{solid}}\right] \quad (2)$$

The negative formation energies in the table indicate that all of the x compositions are structurally stable and synthesizable. The lowest ΔH_f value is at $x = 0.7$ ($\Delta H_f = -0.329$ eV/f.u.).

Another way to determine the stability of a structure is calculating the ratio of the occupied states width to the bonding states width (W_{occ}/W_b), because according to the band filling theory, the stability of a material increases along with the increase (decrease) in the numbers of bonding (anti-bonding) states [45,46]. When this ratio is closer to 1.0, one can observe that the stability increases. Table 1 shows the computed pseudogaps (W_p, the nearest valley to the Fermi level), occupation gaps (W_{occ}), bonding gaps (W_b) and the W_{occ}/W_b ratios for all x compositions. As it can be seen from the table, $W_{occ}/W_b = 0.987$ (for $x = 0.7$) is the closest value to 1.0, which means $W_{0.3}Ru_{0.7}B_2$ is the most stable one as predicted from formation energy calculations above.

Also, the variation of electron numbers (n) at Fermi level is another indicator of the structural stability, so the lowest n value can be expected to refer to the most stable structure. According to Fig. 2, $W_{1-x}Ru_xB_2$ achieves the minimum point at $x = 0.7$ with a value of $n = 0.935$. In consequence of above-stated structural stability calculations, $W_{0.3}Ru_{0.7}B_2$ is found to be the most stable composition among others.

To obtain information about the electronic properties of the $W_{1-x}Ru_xB_2$, partial density of states (PDOS) have been calculated for each x composition, but only illustrated for the most stable $x = 0.7$ composition to save space in the journal (Fig. 3). Hereby, the bonding character demonstrated by the PDOS gives information on hybridization and the orbital character of the states. For

Table 1
Calculated equilibrium lattice parameters (a and c, in Å), Pseudogap (W_p in eV), the width of occupied states (W_{occ} in eV), bonding States (W_b in eV), electron numbers at fermi level (n), formation energies (ΔH_f in eV/f.u), internal parameters (z) for $W_{1-x}Ru_xB_2$.

x	VEC	a	c	W_p	W_{occ}	W_b	W_{occ}/W_b	n	ΔH_f	z
0.1	4.067	2.916	7.686	−0.454	14.293	13.839	1.032	1.152	−0.320	0.542
0.2	4.133	2.908	7.628	−0.611	14.370	13.760	1.044	1.439	−0.306	0.543
0.3	4.200	2.904	7.568	1.183	14.433	15.617	0.924	1.777	−0.292	0.545
0.4	4.267	2.900	7.511	1.088	14.435	15.524	0.930	1.750	−0.296	0.546
0.5	4.333	2.898	7.459	0.915	14.444	15.358	0.940	1.374	−0.301	0.548
0.6	4.400	2.897	7.407	0.498	14.684	15.183	0.967	0.999	−0.315	0.549
0.7	4.467	2.896	7.370	0.194	14.884	15.078	0.987	0.935	−0.329	0.550
0.8	4.533	2.900	7.329	−0.246	15.100	14.854	1.017	1.0467	−0.325	0.551
0.9	4.600	2.905	7.298	−0.505	15.142	14.637	1.034	1.498	−0.311	0.551

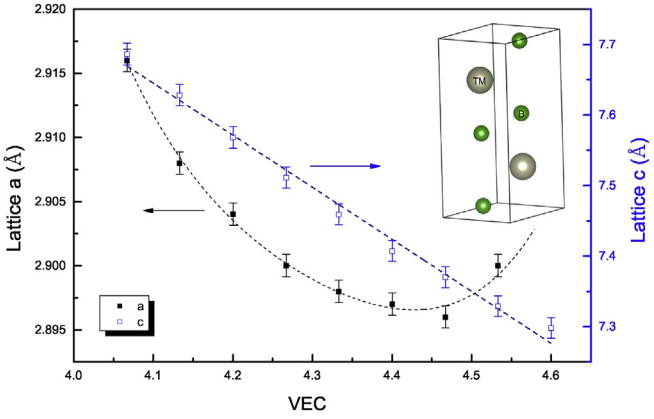

Fig. 1. The variation of lattice parameters (in Å) with respect to *VEC* values for $W_{1-x}Ru_xB_2$.

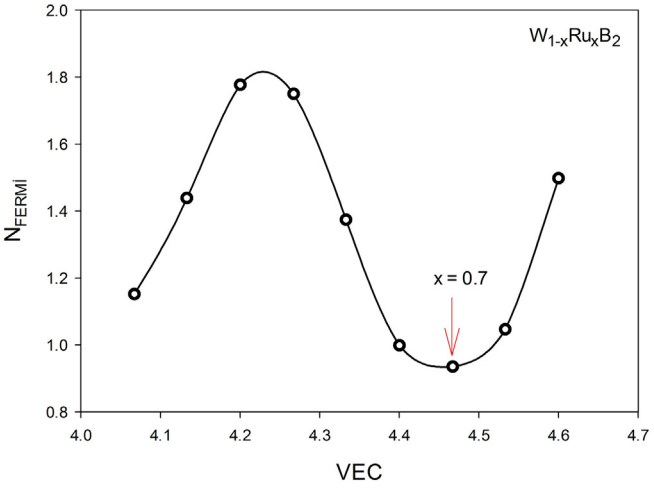

Fig. 2. The variation of electron numbers at Fermi levels with respect to *VEC* values for $W_{1-x}Ru_xB_2$.

$W_{0.3}Ru_{0.7}B_2$, the lowest energy states from −14.30 eV to −7.43 eV are essentially dominated by *s* and *p* orbitals of the compound. The states between −7.43 eV and 4.34 eV consists of *d* and *p* orbitals with a minor presence of *s* states, but when running across the Fermi level, s states almost disappear and only *d*-*p* interaction remains. Between 4.34 eV and 12.55 eV, *d* orbitals nearly lose their active existence and *s*-*p* orbitals arise thoroughly. As seen in the PDOS graphic and before-mentioned *n* values for each *x*, the band structure exhibits a metallic character.

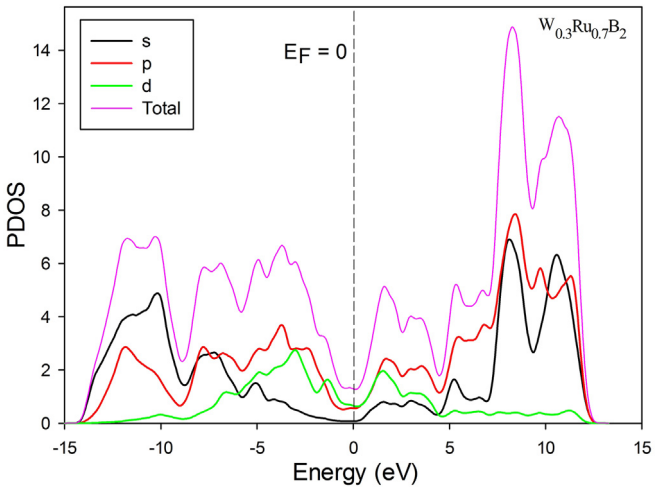

Fig. 3. Calculated partial density of states (PDOS) of $W_{0.3}Ru_{0.7}B_2$.

In order to visualize the nature of the bonding character of $W_{0.3}Ru_{0.7}B_2$, the valence charge density for (110) plane has been displayed in Fig. 4. As can be seen in this figure, electron density between *TM* ($W_{0.3}Ru_{0.7}$) and *B* atoms decreases while it increases between *B* atoms. Also, the structure shows a mixture of both covalent and ionic bonding.

3.2. Elastic and anisotropic properties

The elastic constants have been computed by using the "stress–strain" method implemented in CASTEP code. There are

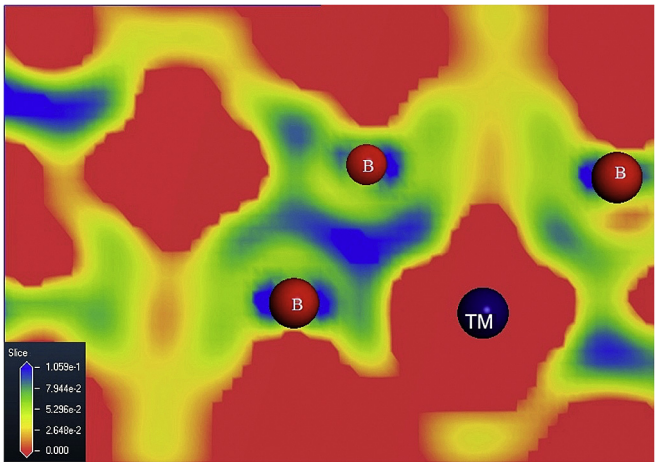

Fig. 4. Calculated charge density of $W_{0.3}Ru_{0.7}B_2$ for (110) plane.

five elastic constants of a hexagonal structure named as C_{11}, C_{12}, C_{13}, C_{33}, and C_{44}; while $C_{66} = (C_{11}-C_{12})/2$. These calculated values given in Table 2 have been plotted for corresponding VEC values in Fig. 5 to visualize all of them easily together. To determine the mechanical stability of the structure, these elastic constants should satisfy the Born-Huang criteria, which is known as $C_{44} > 0$, $C_{11} > |C_{12}|$, $(C_{11} + C_{12})C_{33} > 2C_{13}^2$ [47]. Our results satisfy these stability conditions, suggesting that $W_{1-x}Ru_xB_2$ is mechanically stable for all x compositions. The highest elastic constant is C_{33}, while C_{13} is the lowest one for all x compositions. Also, C_{11} is lower than C_{33}, indicating that $W_{1-x}Ru_xB_2$ is more compressible along the a-axis than c-axes. On the other hand, calculated C_{44} for all x compositions are higher than C_{66} which means that the shear along the (001) plane is relatively easier than the shear along the (100) plane [48].

Bulk (B) and Shear (G) modulus can be obtained from calculated elastic constants using Voigt (V) [49] and Reuss (R) [50] schemes. Within these approximations, B and G values can be found as below:

$$B_V = [2(C_{11} + C_{12}) + 4C_{13} + C_{33})]. \quad (3)$$

$$G_V = (C_{11} + C_{12} + 2C_{33} - 4C_{13} + 12C_{44} + 12C_{66}). \quad (4)$$

$$B_R = \left((C_{11} + C_{12})C_{33} - 2C_{12}^2\right) + 12C_{44}/(C_{11} + C_{12} + 2C_{33} - 4C_{13}). \quad (5)$$

$$G_R = \left\{\left[(C_{11} + C_{12})C_{33} - 2C_{12}^2\right)C_{55}C_{66}\right\}/\left\{3B_VC_{55}C_{66} + \left[(C_{11} + C_{12})C_{33} - 2C_{12}^2\right]^2(C_{55} + C_{66})\right\} \quad (6)$$

It is known that the Voigt bound is obtained by the average polycrystalline moduli based on an assumption of uniform strain throughout a polycrystal and is the upper limit of the actual effective moduli while the Reuss bound is obtained by assuming a uniform stress and is the lower limit of the actual effective moduli. Therefore, the Voigt–Reuss–Hill (VRH) approximation [51] is widely used to make an acceptable estimation of elastic parameters for polycrystalline materials. Here, effective moduli for isotropic polycrystals is derived from the arithmetic mean of the Voigt and Reuss limits:

$$B = (B_V + B_R)/2 \quad (7)$$

$$G = (G_V + G_R)/2 \quad (8)$$

In addition, Young's modulus (E) and Poisson's ratio (ν) can be calculated using the following relations [52]:

$$E = 9BG/(3B + G) \quad (9)$$

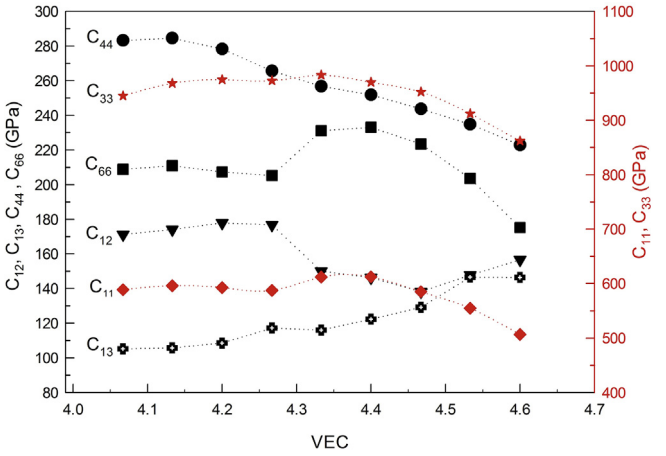

Fig. 5. The variation of C_{ij} (in GPa) with respect to *VEC* values for $W_{1-x}Ru_xB_2$.

$$\nu = (3B-2G)/(2(3B + G)) \quad (10)$$

The calculated Bulk moduli (B), Shear moduli (G), Young's modulus (E), and Poisson's ratio (ν) according to VRH approximation are listed in Table 3. The calculated bulk moduli of $W_{1-x}Ru_xB_2$ increase until $x = 0.6$ and after decrease, but all of them still transcend the ultra-incompressibility threshold (300 GPa). As seen from the table, $W_{0.4}Ru_{0.6}B_2$ is the least compressible material.

The Shear modulus is a measurement of resistance of the material to transverse deformations and its magnitude is directly proportional to C_{44}. In general, high value of Shear modulus is due to the directional bonding between atoms where electron density is geometrically localized, thus more energy is needed to break these bonds [2]. Among the considered compositions, $W_{0.8}Ru_{0.2}B_2$ possesses the highest Shear modulus (267.3 GPa).

B/G ratio is the indicator of ductility or brittleness of a material where values higher than 1.75 refer ductility while lower values indicate brittleness [53]. All of the B/G values in Table 3 are less than 1.75. Hence, $W_{1-x}Ru_xB_2$ behaves in a brittle manner, especially $W_{0.9}Ru_{0.1}B_2$. The same result can also be confirmed by Cauchy pressure calculations. Cauchy pressure is defined as $(C_{12}-C_{66})$ and $(C_{13}-C_{44})$ for hexagonal materials and a positive value of it brings out damage tolerance and ductility of a crystal, while the negative one shows brittleness.

Relatedly, G/B ratio (Pugh's modulus) is the parameter used to determine the bonding character of the atoms in the crystal. If the value of G/B is about 1.1, covalent bonding is more dominant than ionic bonding; for $G/B \approx 0.8$, the opposite is true [54]. All the values in Table 3 are about 0.8 that indicates ionic bonding is dominant in the structure.

The above-stated bonding nature of the $W_{1-x}Ru_xB_2$ is supported by the Poisson's ratio values as well. According to the literature, the

Table 2
Elastic constants (C_{ij}, in GPa) of $W_{1-x}Ru_xB_2$.

X	VEC	C_{11}	C_{12}	C_{13}	C_{33}	C_{44}	C_{66}
0.1	4.067	588.8	171.1	105.2	944.8	283.2	208.8
0.2	4.133	595.9	174.0	105.7	967.9	284.6	210.9
0.3	4.200	592.5	177.8	108.5	974.7	278.3	207.4
0.4	4.267	587.3	176.7	117.3	972.7	265.6	205.3
0.5	4.333	612.1	149.9	116.1	983.0	256.7	231.1
0.6	4.400	612.3	146.2	122.3	969.9	251.8	233.1
0.7	4.467	585.0	138.2	129.2	952.2	243.7	223.4
0.8	4.533	554.8	147.6	146.6	912.1	234.8	203.6
0.9	4.600	506.8	156.5	146.3	862.0	222.8	175.1

Table 3
Calculated bulk modulus (B, in GPa), Shear Modulus (G, in GPa), Young's modulus (E in GPa), Poisson's ratio (ν), and Vicker's Hardness (H_v, in GPa) for $W_{1-x}Ru_xB_2$.

X	VEC	B	G	E	ν	B/G	G/B	H_V
0.1	4.067	316.4	264.4	620.4	0.173	1.197	0.836	40.0
0.2	4.133	321.2	267.3	627.7	0.174	1.202	0.832	40.1
0.3	4.200	323.7	263.3	621.4	0.180	1.230	0.813	38.6
0.4	4.267	324.7	256.3	608.7	0.187	1.267	0.789	36.7
0.5	4.333	324.6	265.6	626.0	0.179	1.222	0.818	39.1
0.6	4.400	325.1	263.1	621.6	0.181	1.236	0.810	38.4
0.7	4.467	317.2	252.9	599.3	0.185	1.254	0.800	36.8
0.8	4.533	315.3	235.9	566.4	0.200	1.34	0.75	32.8
0.9	4.600	300.9	214.3	519.5	0.212	1.404	0.712	29.3

small values about 0.1 correspond to the covalent materials whereas for ionic materials the typical value of ν is 0.25 [54]. In Table 3, all ν values are between 0.1 and 0.25 implying that the bonding character of this structure is a mixture of covalent and ionic bonds, as mentioned before when discussing the charge density map. On the other hand, these values are closer to 0.25, indicating that there is a trend from covalent to ionic contribution to the inter-atomic bonding, especially for higher *Ru* content.

Young's modulus is defined as the ratio of stress to strain and used to provide a measure of the stiffness of the solid. The highest value of Young's modulus (627.7 GPa) is found for the $x = 0.2$ ($VEC = 4.133$) composition, suggesting that $W_{0.8}Ru_{0.2}B_2$ is, relatively, stiffer than that of the other *x* compositions.

As the last parameter in Table 3, hardness has been calculated by using the semi-empirical method based on Pugh's modulus ratio developed by Chen et al. [55]. It is given as;

$$H_V = 2(k^2G)^{0.585} - 3;\ (k = G/B) \tag{11}$$

Here, the parameter k is the Pugh's modulus ratio. According to Table 3, the calculated hardness values decrease as the Ru content increases, but all $W_{1-x}Ru_xB_2$ compounds are still hard materials. Especially, two of them, $W_{0.9}Ru_{0.1}B_2$ and $W_{0.8}Ru_{0.2}B_2$, slightly exceed the superhardness limit ($H_V \geq 40$ GPa). Most of the hardness values in the table are comparable to those of the pure WB2 compound; this makes $W_{1-x}Ru_xB_2$ a good candidate for technological applications [21,22].

The anisotropy of elasticity is another interesting physical parameter of solids that has a great impact on engineering science and crystal physics, including phase transformations, precipitation, dislocation dynamics and microcrack formation [56,57]. Among them, microcrack formation takes special attention due to its effect on the mechanical properties of the material. For this reason, elastic anisotropy studies are quite necessary to understand the mechanism of microcracks in order to increase the hardness of the material [58]. Therefore, firstly, the directional dependence of the linear compressibility, Young's modulus, Shear modulus, and Poisson ratio of $W_{1-x}Ru_xB_2$ are obtained by using ElAM code [59] which is a good analytical tool to calculate and visualize anisotropic elastic properties. Here, the data calculated by using the relations given in Refs. [60,61] have been used to plot three-dimensional (3D) dependence of these properties along crystallographic directions. The 3D elastic anisotropy graphics in Fig. 6 are given only for the most stable $W_{0.3}Ru_{0.7}B_2$ to save space in the journal. It is known that, if a crystal is isotropic, it exhibits a spherical shape in a 3D representation. If there is a deviation from a spherical shape, it indicates the degree of anisotropy [62]. It is clearly seen in Fig. 6 that the $W_{0.3}Ru_{0.7}B_2$ is isotropic at the *xy*-plane, while it is anisotropic at the *xz*- and *yz*-planes. Also, the calculated maximum and minimum values of these 3D graphics are listed in Table 4.

Secondly, anisotropic factors (A_1, A_2, A_3) have been calculated using the following equations given in Ref. [63] in which these equations were mentioned as the most useful ones to provide in-plane phonon-focusing information for hexagonal crystals.

$$A_1 = \frac{C_{44}(C_{11} + 2C_{13} + C_{33})}{\left(C_{11}C_{33} - C_{13}^2\right)} \quad \text{for} \quad [001] \tag{12}$$

$$A_2 = \frac{2C_{44}}{(C_{11} - C_{13})} \quad \text{for} \quad [100],\ (010) \tag{13}$$

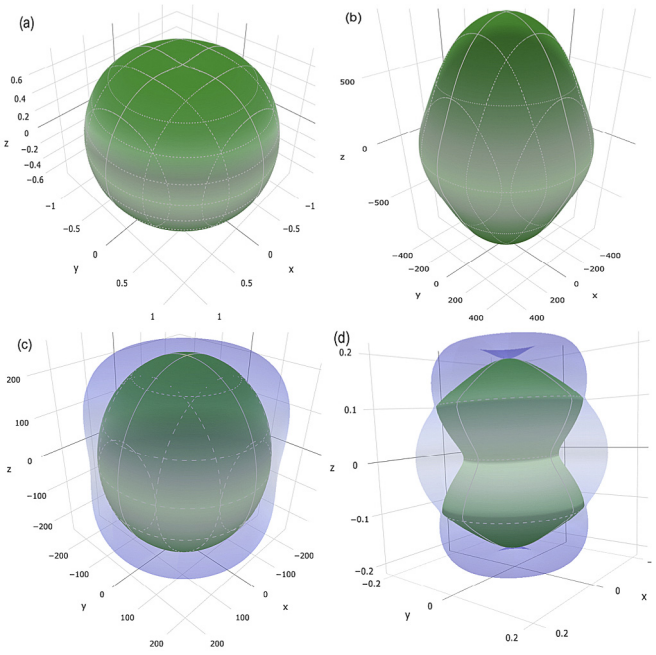

Fig. 6. 3D directional dependence of (*a*) the compressibility (in TPa^{-1}), (*b*) Young's modulus (in GPa), (*c*) Shear modulus (in GPa), and (*d*) Poisson's ratio for $W_{0.3}Ru_{0.7}B_2$.

Table 4
Maximum and minimum values of Young's modulus (E_{max} and E_{min}, in GPa), linear compressibility (β_{max} and β_{min}, TPa^{-1}), Shear moduli (G_{max} and G_{min}, in GPa), and Poisson's ratio (ν_{max} and ν_{min}) of $W_{1-x}Ru_xB_2$.

X	VEC	Linear Comp.		Young's Modulus		Shear Modulus		Poisson Ratio	
		β_{min}	β_{max}	E_{min}	E_{max}	G_{min}	G_{max}	ν_{min}	ν_{max}
0.1	4.067	0.790	1.207	533.0	915.7	208.8	305.8	0.081	0.276
0.2	4.133	0.773	1.193	539.2	938.8	210.9	311.3	0.079	0.278
0.3	4.200	0.761	1.191	533.1	944.1	207.4	309.3	0.079	0.285
0.4	4.267	0.740	1.195	527.1	936.7	205.3	303.7	0.086	0.284
0.5	4.333	0.734	1.200	567.2	947.6	231.1	318.6	0.091	0.226
0.6	4.400	0.728	1.201	567.1	930.5	233.1	314.3	0.098	0.236
0.7	4.467	0.709	1.256	541.8	906.1	223.4	299.1	0.107	0.241
0.8	4.533	0.684	1.281	502.3	850.9	203.6	273.5	0.123	0.240
0.9	4.600	0.701	1.353	446.0	797.4	175.1	246.9	0.123	0.273

$$A_3 = \frac{2C_{44}}{(C_{33} - C_{13})} \quad \text{for} \quad [001],\ (010) \tag{14}$$

Here, the [*ijk*] and (*ijk*) represents symmetry axis and plane. For a completely isotropic material, A_1, A_2, A_3 values are one, while a deviation from this value refers to an elastic anisotropy. Also, positive smaller or grater values of A_2 and A_3 indicate in-plane focusing or defocusing, respectively. The calculated anisotropic factors are given in Table 5. All the values in the table deviate from one, referring to the anisotropic mechanic character of all x compositions. We have also calculated the universal anisotropy index (A^U) and percent elastic anisotropy in shear and compression (A_G, A_B) by the following common relation given in Refs. [64,65].

$$A^U = 5(G_V/G_R) + (B_V/B_R) - 6 \tag{15}$$

$$A_G = (G_V - G_R)/(G_V + G_R) \tag{16}$$

$$A_B = (B_V - B_R)/(B_V + B_R) \tag{17}$$

Table 5
Shear anisotropic factors (A_1, A_2, and A_3), the percentage (in %) of anisotropy in the compression and shear (A_B and A_G), and universal anisotropic index (A^U) for $W_{1-x}Ru_xB_2$.

X	VEC	A_1	A_2	A_3	A_B	A_G	A^u
0.1	4.067	0.906	1.171	0.675	1.3	2.5	0.505
0.2	4.133	0.893	1.161	0.660	1.4	2.6	0.521
0.3	4.200	0.878	1.150	0.643	1.5	2.7	0.564
0.4	4.267	0.855	1.130	0.621	1.6	2.6	0.593
0.5	4.333	0.797	1.035	0.592	1.7	1.9	0.459
0.6	4.400	0.795	1.028	0.594	1.7	1.7	0.453
0.7	4.467	0.810	1.069	0.592	2.1	1.7	0.480
0.8	4.533	0.853	1.150	0.613	2.3	1.8	0.572
0.9	4.600	0.891	1.236	0.622	2.4	2.3	0.711

The obtained results (A^U, A_G, and A_B) can be seen in Table 5. For isotropic materials, the universal index and percent anisotropy in shear and compression are taken as zero. A value of zero (B_R=B_V) is associated with elastic isotropy, while a value of 100% is associated with the largest anisotropy [66].

4. Summary and conclusions

The effect of *Ru* doping on the structural, electronic, elastic, and anisotropic elastic properties of the WB_2 compound has been investigated by using the first-principles DFT calculations. In these calculations, no effect of spin-polarization has been observed.

Among nine considered doping ratios, $W_{0.3}Ru_{0.7}B_2$ composition has been found to be the most stable one. This structure is metallic and has a mixture of covalent and ionic bonds. The calculated elastic constants have also indicated that all $W_{1-x}Ru_xB_2$ compositions are mechanically stable. According to our results, all of the structures are in a brittle and stiffer manner.

When compared, bulk and Shear modulus of $W_{1-x}Ru_xB_2$ have been found to be higher than that of the host WB_2 and RuB_2 compounds. Moreover, the Poisson's ratio is closer to 0.1, which shows that the *Ru* additive cause the covalent bonds in the structure to be more dominant. Thus, it has been found that all *x* compositions are harder than the host compounds. Particularly, $x = 0.1$ and $x = 0.2$ compositions slightly exceed the superhardness limit. These values are also better than that of other TM-borides such as MoB_2, OsB_2. As a result, it can be said that *Ru* doping improves the mechanical properties of WB_2, which is desirable for super-hardness applications.

According to the 3D elastic anisotropy graphics and calculations, $W_{1-x}Ru_xB_2$ compositions are isotropic at the *xy* plane, while they are anisotropic at the *xz* and *yz* planes. This knowledge is necessary when controlling the microcrack formation in the structure. Also, it may be important for applications that require directional dependence of the physical properties.

Consequently, we hope that these systematic calculations and analysis of the structural, electronic and mechanical properties of $W_{1-x}Ru_xB_2$ reported here will be useful in the future design of new materials with borides.

Acknowledgment

This work was supported by the Turkish Prime Ministry State Planning Agency under projects no. 2011K120290.

References

[1] R.B. Kaner, J.J. Gilman, S.H. Tolbert, Mater. Sci. 308 (2005) 1268.
[2] M.T. Yeung, R. Mohammadi, Richard B. Kaner, Annu. Rev. Mater. Res. 48 (2016) 465.
[3] R.W. Cumberland, M.B. Weinberger, J.J. Gilman, S.M. Clark, S.H. Tolbert, R.B. Kaner, J. Am. Chem. Soc. 127 (2005) 7264.
[4] H.Y. Chung, M.B. Weinberger, J.B. Levine, A. Kavner, J.M. Yang, S.H. Tolbert, R.B. Kaner, Science 316 (2007) 436.
[5] L.P. Ding, P. Shao, F.H. Zhang, C. Lu, L. Ding, S.Y. Ning, X.F. Huang, Inorg. Chem. 55 (2016) 7033.
[6] H. Euchner, P.H. Mayrhofer, Thin Solid Films 583 (2015) 46.
[7] J.B. Levine, S.H. Tolbert, R.B. Kaner, Adv. Funct. Mater 19 (2009) 3519.
[8] Y. Liang, Y. Gou, X. Yuan, Z. Zhong, W. Zhang, Chem. Phys. Lett. 580 (2013) 48.
[9] Q. Li, D. Zhou, W. Zheng, Y. Ma, C. Chen, Phys. Rev. Lett. 115 (2015) 185502.
[10] M.T. Yeung, J. Lei, R. Mohammadi, C.L. Turner, Y. Wang, S.H. Tolbert, R.B. Kaner, Adv. Matt. 28 (2016) 6993.
[11] A. Simunek, Phys. Rev. B 80 (2009) 060103(R).
[12] T. Moscicki, J. Radziejewska, J. Hoffman, J. Chrzanowska, N. Levintant-Zayonts, D. Garbiec, Z. Szymanski, Ceram. Int. 41 (2015) 8273.
[13] I.R. Shein, A.L. Ivanovskii, J. Condens. Matter. 20 (2008) 415218.
[14] W. Zhou, H. Wu, T. Yildirim, Phys. Rev. B 76 (2007) 184113.
[15] R. Mohammadi, C.L. Tuner, M. Xie, M.T. Yeung, A.T. Lech, S.H. Tolbert, R.B. Kaner, Chem. Mater. 28 (2016) 632.
[16] H. Duschanek, P. Rogl, Phase Equilib. 16 (1995) 50.
[17] E. Zhao, J. Meng, Y. Ma, Z. Wu, Phys. Chem. Chem. Phys. 12 (2010) 13158.
[18] Y. Liang, X. Yuan, W. Zhang, Phys. Rev. B 83 (2011) 220102.
[19] H. Dong, S.M. Dorfman, Y. Chen, H. Wang, J. Wang, J. Qin, D. He, T.S. Duffy, J. Appl. Phys. 111 (2012) 123514.
[20] Q. Li, D. Zhou, W. Zheng, Y. Ma, C. Chen, Phys. Rev. Lett. 110 (2013) 136403.
[21] X.Y. Cheng, X.Q. Chen, D.Z. Li, Y. Y Li, Acta Cryst. C70 (2014) 85.
[22] M. Mazdziarz, T. Moscicki, Mater. Chem. Phys. 179 (2016) 92.
[23] G. Akopov, M.T. Yeung, C.L. Turner, R. Mohammadi, R.B. Kaner, J. Am. Chem. Soc. 138 (2016) 5714.
[24] S. Feng, X. Li, L. Su, H. Li, H. Yang, X. Cheng, Solid State Comm. 245 (2016) 60.
[25] X. Cao, C. Wang, L. Shi, H. Yang, X. Xue, H. Li, Int. J. Refract. Metals Hard Mater. 41 (2013) 597.
[26] G. Surucu, K. Colakoglu, E. Deligoz, Y.O. Ciftci, Solid State Commun. 171 (2013) 1.
[27] Q.F. Gu, G. Krauss, W. Steurer, Adv. Mater. 20 (2008) 3620.
[28] X.P. Du, Y.X. Wang, Phys. Status Solidi (RRL) 3 (2009) 106.
[29] X.Y. Zhang, Z.W. Chen, C.Z. Fan, M.Z. Ma, Q. Jing, R. Liu, Phys. Status Solidi (RRL) 3 (2009) 299.
[30] Y. Tu, Y. Wang, Solid State Commun. 151 (2011) 238.
[31] Y. Wang, T. Yao, L.M. Wang, J. Yao, H. Li, J. Zhang, H. Gou, Dalton Trans. 42 (2013) 7041.
[32] X. Zhang, E. Zhao, Z. Wu, K. Li, Q. Hou, Comput. Mater. Sci. 95 (2014) 377.
[33] Z. Li, D. Zheng, Z. Ding, Y. Li, B. Yao, Y. Li, X. Zhao, G. Yu, Y. Tang, W. Zheng, X. Liu, Mater. Res. Bull. 74 (2016) 188.
[34] J.J. Gilman, R.W. Cumberland, R.B. Kaner, Int. J. Refract. Metals Hard Mater. 24 (2006) 1.
[35] P. Rogl, H. Nowotny, F. Benesovsky, Monatshefte Chemie 101 (1970) 27.
[36] M.D. Segall, P.J.D. Lindan, M.J. Probert, C.J. Pickard, P.J. Hasnip, S.J. Clark, M.C. Payne, J. Phys. Condens. Mater 14 (2002) 2717.
[37] W. Zhu, H. Xiao, J. Comput. Chem. 29 (2008) 176.
[38] J.P. Perdew, K. Burke, M. Ernzerhof, Phys. Rev. Lett. 77 (1996) 3865.
[39] J.P. Perdew, J.A. Chevary, S.H. Vosko, K.A. Jackson, M.R. Pederson, D.J. Singh, C. Fiolhais, Phys. Rev. B 46 (1992) 6671.
[40] D. Vanderbilt, Phys. Rev. B 41 (1990) 7892.
[41] L. Bellaiche, D. Vanderbilt, Phys. Rev. B 61 (2000) 7877.
[42] H.J. Monkhorst, J.D. Pack, Phys. Rev. B 13 (1976) 5188.
[43] X. Hao, Y. Xu, Z. Wu, D. Zhou, X. Liu, X. Cao, J. Meng, Phys. Rev. B 74 (2006) 224112.
[44] L. Vegard, Z. für Phys. 5 (1921) 17.
[45] J.H. Xu, T. Oguchi, A.J. Freeman, Phys. Rev. B 35 (1987) 6940.
[46] J.H. Xu, A.J. Freeman, Phys. Rev. B 40 (1989) 11927.
[47] Z. Wu, E. Zhao, H. Xiang, X. Hao, X. Liu, J. Meng, Phys. Rev. B 76 (2007) 054115.
[48] V.V. Bannikov, I.R. Shein, A.L. Ivanovskii, Phys. B 407 (2012) 271.
[49] W. Voight, Lehrb. Krist. 29 (1928) (Leipzig: Teubner).
[50] A. Reuss, Zeitschrift fur Angewandte Mathematik und Mechanik, 1929, p. 949.
[51] R. Hill, Proc. Phys. Soc. Lond. 65 (1952) 349.
[52] S.Q. Wu, Z.F. Hou, Z.Z. Zhu, Solid State Commun. 143 (2007) 425.
[53] S.F. Pugh, Phil. Mag. Ser. 45 (1954) 823.
[54] V.V. Bannikov, I.R. Shein, A.L. Ivanovskii, Phys. Stat. Sol. (RRL) 1 (2007) 89.
[55] X.Q. Chen, H. Niu, D. Li, Y. Li, Intermetallics 19 (2011) 1275.
[56] M. Xing, B. Li, Z. Yu, Q. Chen, J. Phys. Chem. Solid 91 (2016) 106.
[57] R. Hao, X. Zhang, J. Qin, J. Ning, S. Zhang, Z. Niu, M. Ma, R. Liu, RSC Adv. 5 (2015) 77399.
[58] X. Hao, Y. Xu, Z. Wu, D. Zhou, X. Liu, J. Meng, J. Alloys Compd. 453 (2008) 413.
[59] A. Marmier, Z.A.D. Lethbridge, R.I. Walton, C.W. Smith, S.C. Parker, K.E. Evans, Comput. Phys. Commun. 181 (2010) 2102.
[60] U.F. Ozyar, E. Deligoz, K. Colakoglu, Solid State Sci. 40 (2015) 92.
[61] A.U. Ortiz, A. Boutin, A.H. Fuchs, F.X. Coudert, J. Chem. Phys. 138 (2013) 174703.
[62] N. Guechi, A. Bouhemadou, R. Khenata, S. Bin-Omran, M. Chegaar, Y. Al-Douri, A. Bourzami, Solid State Sci. 29 (2014) 12.
[63] H. Fu, W.F. Liu, Y. Ma, T. Gao, J. Alloys Comp. 506 (2010) 22.
[64] N. Miao, B. Sa, J. Zhou, Z. Sun, Comp. Mater. Sci. 50 (2011) 1559.
[65] S.I. Ranganathan, M.O. Starzewski, Phys. Rev. Lett. 101 (2008) 055504.
[66] D.H. Chung, W.R. Buessem, Anisotropy in Single Crystal Refractory Compound, in: F.W. Vahldiek, S.A. Mersol (Eds.), Plenum, New York, 1968, p. 328.